39th AIAA/ASME/SAE/ASEE Joint Propulsion Conference and Exhibit
20-23 July 2003, Huntsville, Alabama

AIAA 2003 - 5082

Direct Numerical Simulation of Sandwich and Random-Packed Propellant Combustion

R. Cazan and S. Menon
School of Aerospace Engineering
Georgia Inst. of Technology
Atlanta, GA 30332 USA
(radu_cazan, suresh.menon)@ae.gatech.edu
http://www.ccl.gatech.edu

39th AIAA/ASME/SAE/ASEE
Joint Propulsion Conference
20-23 July 2003 / Huntsville, AL

Direct Numerical Simulation of Sandwich and Random-Packed Propellant Combustion

R. Cazan* and S. Menon†
School of Aerospace Engineering
Georgia Inst. of Technology
Atlanta, GA 30332 USA
(radu_cazan, suresh.menon)@ae.gatech.edu
http://www.ccl.gatech.edu

This paper presents the formulation and results for a direct numerical simulations (DNS) of solid propellant combustion. Finite-rate kinetics of Ammonium Percholate (AP) decomposition and AP combustion with Binder is simulated in this study with full resolution of the flame zone. Both the solid phase and the gas phase are simulated with two-dimensional surface regression. A new numerical approach to capture the motion of the burning surface is developed and used in this study. We analyze the burning of various sandwich and randomly packed structures. Simulations show that a complex flame structure consisting of premixed and non-premixed type flamelets is present above the burning surface. Issues related to using this DNS approach for more complex burning cases, especially at high pressure are also addressed.

1 Introduction

Nearly all missiles are propelled by solid propellant rocket motors. The current state-of-the-art propellant mixtures used in these motors, typically, particles of ammonium perchlorate (AP) and aluminum (Al) in a fuel binder, have been created using an extensive empirical database that correlates propellant mixture to burn rate. This database is a result of many years of parametric experimental study but is limited by the experimental range of conditions that could be simulated in the laboratory. As a result, future improvements and development of next generation high-energetic propellants is very difficult since the current data cannot be reliably extended to other operational space, for example, higher pressure. For example, current empirical data is limited to propellant burning up to 200 atm. Much higher pressures (e.g., 550-1000 atm) of propellant combustion are of considerable interest since it is estimated that nearly 60-70 percent of the total volume of the current missile is made up of the propellant. Thus, a significant increase in propellant combustion pressure and the use of highly energetic fuel mixtures could drastically reduce the volume and weight of the propellant needed without compromising payload and performance capabilities.

In addition, improvements in the propellant mix and the use of high-pressure combustion will also reduce the size of the missile. However, development of such high energetic, high-pressure propellant is very difficult since parametric studies in the laboratory are very difficult (if not impossible) and likely to be very expensive. The reliability of the empirical rules (developed from lower pressure experiments) at higher pressure is not known since there is no in-depth understanding of the actual propellant combustion process. Furthermore, even though there is now a wealth of "empirical" knowledge on how certain ingredients (i.e., propellant mix) interact and changes the burn rate, there still are many unresolved issues regarding the burning rate of these propellants. For example, certain high propellant formulation (i.e., mixture) exhibits a burning behavior called "plateau" burning. This refers to a pressure in-sensitive burning rate within one or more pressure ranges. This behavior is of considerable interest since it can help provide stable solid rocket motor design and advantageous performance, provided this plateau burning can be produced at the desired pressure and burning rate in a formulation that meets also the other requirements for manufacture, mechanical properties, safety, etc. Analysis of data has shown that plateau burning can be highly dependent on many parameters, among them, the relative proportion of coarse and fine ammonium perchlorate (AP), particle size, amount and kind of binder, and the amount and kind of additives such as transition metal oxides. So far, it has been difficult to exploit this behavior using experimental formulation and no analytical or computational model currently exists that can be used to understand the dynamical interaction between the various factors involved in AP-Hydrocarbon (HC) combustion process.

The peculiarities even in the currently employed propellants are not yet fully explored since no analytical or modeling capability currently exists. Furthermore, the development of very high-pressure high energetic propellant formulation critically requires that a fundamental understanding of the basic physics of solid propellant combustion be achieved.

At present, the only viable option is to develop and employ a first principle DNS capability that includes all

*Graduate Student; Student member, AIAA
†Associate Fellow, AIAA; Corresponding Author

the dynamical physics (surface structure, propellant packing, surface kinetics and regression, flame structure, etc.) without making any a priori assumptions and/or approximations. Once such a model has been validated against existing database (which is not a trivial issue since chemical kinetics for propellant combustion is not very well known), it could be utilized to investigate performance of high-pressure propellant mixtures. Note that, even though DNS is computationally very demanding, the alternate approach of experimental parametric studies is expensive (if not impossible) economically.

Several attempts at modelling have been reported in the recent years, for example, sandwich structures[1] and random 3D packing.[2] In these studies compressibility effects were ignored, parallel flow (Oseen aproximation) was assumed and flow-chemistry was decoupled. These assumptions may not be directly applicable in the surface region where the temperature gradients are large and the surface is irregular. Also decoupling the flow and the chemical reactions may lead to missing the effects of the AP particle size on burn rates which is the goal of the present simulation.

In this paper, the results of our DNS studies using a fully compressible solver is discussed. Flow-chemistry is fully coupled, as is the gas and the solid phase in this study. Finite-rate kinetics using global kinetics (which is perhaps the only major assumption here) is employed primarily because detailed mechanism is currently not available.[1]

2 Technical Approach

In DNS all scales of motion have to be fully resolved using a highly accurate simulation model. Here, a fully compressible finite-volume scheme that is nominally second-order accurate in both space and time is employed. A fourth-order accurate scheme is also available,[3] but is not used in the present study. Furthermore, although both two-dimensional (2D) and three-dimensional (3D) version of this code are available, only 2D DNS is carried out in this paper. This is considered acceptable at present since the goal of this study is to develop the fully coupled methodology and to demonstrate its application. For sandwich structures with spanwise extent very large relative to the cross plane this 2D approximation is reasonable; however, for randomly packed propellant, 3D effects could be significant. Future simulations will address 3D effects.

The governing equations for the flow field are the conservation of mass, momentum, total energy, and chemical species for a compressible, multi-species, reacting fluid:

$$\begin{cases} \frac{\partial \rho}{\partial t} + \frac{\partial \rho u_i}{\partial x_i} = 0 \\ \frac{\partial \rho u_i}{\partial t} + \frac{\partial}{\partial x_j}\left[\rho u_i u_j + p\delta_{ij} - \tau_{ij}\right] = 0 \\ \frac{\partial \rho E}{\partial t} + \frac{\partial}{\partial x_i}\left[\left(\rho E + p\right)u_i + q_i - u_j\tau_{ji}\right] = 0 \\ \frac{\partial \rho Y_m}{\partial t} + \frac{\partial}{\partial x_j}\left[\rho Y_m u_j + \rho V_{j,m}\right] = \rho\dot{w}_m, m = 1, N \end{cases} \quad (1)$$

where ρ is the mass density, p is the pressure, E is the total energy per unit mass, u_i is the velocity vector and δ_{ij} is the Kronecker function. Also, q_i is the heat flux vector given in Fourier's form: $q_i = -k_g \partial T/\partial x_i$ where the gas thermal conductivity k_g is a function of temperature T chosen to match experimental results:[1] $k_g = 1.08 \times 10^{-4} T + 0.0133$ (W/mK). Finally, Y_m is the mass fraction of species m, $V_{i,m}$ is the i-th diffusion velocity of species m, and $\dot{w}_m$ is the mass reaction rate per unit volume. Newtonian viscous fluid with stress tensor $\tau_{ij} = \mu\left(\partial u_i/\partial x_j\right) - \frac{2}{3}\mu\left(\partial u_k/\partial x_k\right)\delta_{ij}$ is simulated in this study. The molecular viscosity coefficient $\mu = k_g Pr/c_p$ ($Pr = 1$) is obtained assuming unit Prandlt number and assuming that the specific heats, molecular weights and diffusion coefficients are the same for all species. These assumptions are employed at present due to lack of data on these transport properties for the species in our study but is not a model restriction and can be changed when experimental data becomes available.

The pressure is determined from the state equation for a perfect gas mixture: $p = \rho T \sum_{m=1}^{N} Y_m R_u/W_m$ where T is the temperature, R_u is the universal constant and W_m the individual molecular weight (0.034 Kg/mol).[1] The total energy per unit volume is $\rho E = \rho(e + \frac{1}{2}u_k^2)$ where e is the internal energy per unit mass is given by $e = \sum_{m=1}^{N} Y_m h_m - p/\rho$ and h_m is the individual enthalpy. The diffusion velocities are assumed Fickian, i.e., $V_{i,m} = (-D_m/(\partial Y_m/\partial x_i))$ where D_m is the mixture averaged molecular diffusion coefficient. The caloric equation of state is:

$$h_m = \Delta h^0_{f,m} + \int_{T^0}^{T} c_{p,m}(T)dT \quad (2)$$

where $\Delta h^0_{f,m}$ is the standard heat of formation at temperature T^0 and $c_{p,m}$ (= 1255 J/Kg K)[1] is the individual specific heat at constant pressure. The species mass fractions are constrained by $\sum_{m=1}^{N} Y_m = 1$. The diffusion velocities are constrained by $\sum_{m=1}^{N} V_{i,m} = 0$.

2.1 Chemical Mechanism

Four chemical species are considered: AP, AP decomposition products, binder and the products of AP decomposition products/binder flame. The chemical model includes two reactions: gaseous AP decomposition and reaction between AP decomposition products and gaseous binder. The chemical equations are:

$$AP \rightarrow AP\ decomposition\ products\ (APd)$$

$$\beta\ APd + binder\ (b) \rightarrow final\ products\ (p)$$

where $\beta = 8$ is the stoichiometric coefficient.

The reaction rates are:

$$R_1 = D_1 P_0^{n_1} [AP]\ exp\{-E_1/R_u T\}$$

$$R_2 = D_2 P_0^{n_2}\ [APd]\ [b]\ exp\{-E_2/R_u T\}$$

where [AP], [APd] and [b] are the concentrations and D_i, n_i and E_i are chosen to match experimental results.[1] The data used are:

$D_1 = 2.234 \times 10^7$; $n_1 = 1$; $E_1/R_u = 8000K$

$D_2 = 1.105 \times 10^7$; $n_2 = 1$; $E_2/R_u = 11000K$

The standard heats of formation are chosen such that the heat release for AP decompositon reaction is 138.6 Kcal/Kg and the heat release for APd-binder reaction is 3675.9 Kcal/Kg.

It should be pointed out that this chemical mechanism is very simplistic and does not include any radical pathways. However, at present it is not clear what is a good mechanism since data in this arena is grossly lacking.

2.2 Gas Phase Boundary Conditions

The gas phase flow equations are solved subject to proper boundary conditions. At the outflow, characteristic based outflow conditions[4] are imposed while the side boundaries are periodic. At the solid surface the boundary condition is determined by the surface condition which is changing due to surface burning and regression. The implementation of this boundary condition requires solution of the solid phase thermal transport and proper characterization of the surface regression process. These features are discussed in the next two sections.

For the gas flow at the solid surface, the mass, momentum, energy and species fluxes are specified at the surface as boundary conditions (they are functions of the surface temperature). The fluxes are Eulerian as there is no species diffusion through the solid, the viscous heating is very small compare to the reaction terms, and there is no boundary layer effect as the gas is basically injected normal to the surface. Due to the irregular surface (see further discussion below) it is difficult to compute the tangential fluxes, so only the streamwise fluxes are specified at the surface. Two possible cases are shown in Figs. 1a and 1b. The information will reach the neighboring cell in two time steps. Since the time step is very small ($8 * 10^{-10}$ *sec*), there is no significant change at the surface for a relatively long time (e.g., around 100 time steps) and therefore, the cells close to the surface reach a quasi-steady state, so the tangential effect will be felt most of the time. The only exception is in the random package case, when the surface switches between AP and binder. However, even in this case, the transient phase will not last significantly compared to the time the surface spends in a cell (between 50,000 and 100,000 time steps). Detailed analysis of the results has shown that this approach does not introduce any numerical error or instabilities.

A proper validation of this method using idealized conditions has not yet been conducted and is also very difficult due to the nature of the present problem. Most ideal test cases used to validate cut cell methods[5] are designed to simulate a moving fixed-shape surface using mass conservation, whereas in the present case, the surface is moving arbitrarily in each cell and there is surface mass injection (sublimation of the solid phase). Nevertheless, this is an issue for further investigation.

Finally, the species concentrations at the surface boundary are: (a) on the AP side $Y_{AP} = 1$ and the rest $Y_i = 0$ and (b) on the binder side $Y_b = 1$ and the rest $Y_i = 0$. There is no need for Newmann boundary conditions at the surface since the species fluxes specified at the surface do not include the diffusion term.

2.3 Solid Phase Thermal Transport Model

The gas phase processes occur above the solid propellant surface and in order to capture the proper dynamics, the heat transport in the solid phase and the surface regression during combustion both have to be simulated with equally high resolution. For the solid phase, the energy equation:

$$c_{p,m}\rho_{c,m}\frac{\partial T}{\partial t} = \frac{\partial}{\partial x_i}(k_{c,m}\frac{\partial T}{\partial x_i}) \tag{3}$$

for the temperature in the solid phase is solved in 2D using a second-order scheme. Here, the thermal conductivity coefficients $k_{c,m}$ and the densities $\rho_{c,m}$ for the AP and the binder are chosen to match experimental data.[1] In particular, for AP: $k_{c,AP} = 0.405W/mK$; $\rho_{c,AP} = 1950Kg/m^3$ and for binder: $k_{c,b} = 0.276W/mK$; $\rho_{c,b} = 920Kg/m^3$. This equation is solved subject to boundary conditions on the surface (which is regressing). The solid matrix, at the cold end, has a constant temperature which is specified and the side boundaries are periodic. The surface interface balance conditions are described below.

2.4 The Solid/Gas Interface Balance

The mass flow rate of the gas from the solid surface is determined by the rate at which solid phase is converted to gas. This flow rate is determined as $M = \rho_{c,m} r_m$, where r_m is the surface regression rate and $\rho_{c,m}$ is the solid phase density. The gas velocity at the solid/gas interface V is normal to the 2D solid surface (see Fig. 3) and is determined from the regression rate by enforcing conservation of mass. Thus, $V = M/\rho_{gas}$. Once the surface normal velocity V is known, the two Cartesian gas velocity components (u and v) are determined by projecting V on to the x and y axes.

The energy balance at the interface is given by

$$k_{c,m}\frac{\partial T}{\partial x_i} = k_g\frac{\partial T}{\partial x_i} - Q_m M \tag{4}$$

where $Q_m M$ is the term that accounts for the pyrolysis endothermic losses. The value for Q_m for AP and binder are matched to experimental data:[1] $Q_{AP} = 4.2 \times 10^5 (J/Kg)$ and $Q_b = 2.0 \times 10^5 (J/Kg)$. This equation gives the surface temperature at every instant of time. This equation is applied perpendicular to the surface. The heat flux in the solid and the gas phase are computed using points situated at Δx distance from the surface. The temperature in these points is determined by interpolation, using a second-order polynomial $ax + by + cxy + d$. The system is solved using the Gauss algorithm.

2.5 Surface Regression Model

The surface regression model is critical since both the phases are coupled at the surface and proper surface regression is needed to capture the burning rate. Many methods have been used in the past to simulate surface regression. In most cases, the grid is aligned to the surface and surface

regression involves moving grids. Although such methods are very accurate, they are expensive and also have some fundamental limitation when the surface is highly complex 3D shape that changes from cell to cell. An alternate methodology involves using a fixed Cartesian grid and allowing the physical surface to move on this fixed grid. The location of the surface is determined by the surface intersection in the cell and surface boundary conditions are used to enforce appropriate boundary conditions. Cut-cell methods[5] have been developed and demonstrated in the past. Here, we employ a variant of this method. However, as noted earlier, for the present application a new approach is needed due to the presence of surface mass injection.

In the present approach, the surface position is tracked inside all the relevant finite volume cells. For a cell containing the surface, the volume of the cell is the volume of the fluid in that cell. In order to avoid small cell volumes (which would create numerical instability and restrict time-step), a restriction is enforced whereby, when the fluid volume in a cell is smaller than 50% of the original volume, then this volume is added to the next fluid cell. When the fluid volume exceeds 50% of the original volume, a new cell is added to the fluid domain. The volume of the new cell is equal to the fluid volume of the cell and the previous oversized cell regains its original volume. This implementation is only along the surface of the propellant and past studies have shown that is approach does not create any significant spurious diffusion when high resolution is employed (which is the case here).

This method of surface motion has been validated by tracking the motion of a prescribed surface shape. Figure 2 shows the motion of a sinusoidal surface moving at a fixed prescribed rate. The surface is undisturbed (i.e., undistorted) and moves at the exact speed at all locations. Analysis of these results (and others) show that in order to obtain accurate results, the resolution should be such that the distance between the surface position in consecutive cells is not much larger than a cell width. In the present DNS study this is easily enforced.

The solid surface position is given by the surface intersection with the centerlines parallel to x axis (streamwise) as shown in Fig. 3. The intersection with each centerline is a single valued variable x_{surf}. The evolution of x_{surf} is given by the streamwise projection of the regression normal to the surface:[1]

$$\frac{\partial x_{surf}}{\partial t} = r_m \sqrt{1 + \frac{\partial x_{surf}}{\partial y}} \tag{5}$$

where r_m is the regression rate of the solid. However, the angle of the perpendicular is an average of the angles formed by the two lines intersecting at the center Fig. 3b. In the present case, the resolution is high enough so that the surface is smooth and the two lines have almost the same angle.

In the case of a point of inflection (which may occur at the AP-binder interface) the velocity vectors will point at each other, as shown in Fig. 3a, and some modification is necessary. This configuration is not physical. It is impossible to have velocities with opposite signs at the boundary between AP and binder. In the real case, there are scales of motion down to the molecular level and therefore, transition from AP to binder will be smooth and continuous with no jump in velocity and temperature. However, in a numerical simulation (even in a DNS) the resolution cannot be made infinitely small and there is a compromise between the smallest resolved scale and computational effort involved. In the present case, the grid resolution is $2\mu m$ and thus, scales smaller that $2\mu m$ are not resolved. The implication is that if the AP-binder interface is smaller than this size it cannot be resolved.

Also, a new strategy is necessary because the regression rate is a function of the nature of the surface (if it is AP or binder). A cell can be either AP or binder. If the surface is tracked through the intersection with the grid, the proprieties of the interface between AP and binder can not be computed either with AP or binder formulas (Fig. 3a).

The surface has the tendency to smoothen anyway due to burning and regression, so this discontinuity persists only in some isolated cases. The surface spends about 50000 time steps or more in a cell so the surface has time to smoothen.

The regression rates for AP and binder (mm/s) are given by pyrolysis laws determined experimentaly:[1]

$$r_{AP} = A_{AP}\, exp\{-E_{AP}/R_u T_{surf}\} \tag{6}$$

$$r_b = A_b\, exp\{-E_b/R_u T_{surf}\} \tag{7}$$

where the parameters A_i and E_i are for AP and binder, respectively:[1] $E_{AP} = 22(kcal/mol)$, $A_{AP} = 7.9 \times 10^{-9}(m/s)$, and $E_b = 15(kcal/mol)$, $A_b = 7.5 \times 10^{-7}(m/s)$.

3 Results and Discussion

Two types of test problems have been simulated using the DNS code to demonstrate the ability of the solver. The first case is a simple setup of the sandwich between AP and binder. This configuration has been extensively studied experimentally.[6] The second test case is a more complex (and more realistic) setup of arbitrary packing of AP (of various sizes) in binder. Here, we will focus on some of the key results obtained in these studies to highlight the accuracy and the ability of the developed model.

All simulations were conducted using a highly optimized parallel simulation code. High scalability and efficiency is achieved in this code using domain decomposition. Typical simulation employed a resolution of 200 x 240 grid points (resolution depends on the test case) and required a storage of 159 MB and around 2700 single processor hours on Compaq SC 45 to complete a simulation. However, note that these are transient simulations and the amount of time depends for how long surface burning is simulated. Typically, "steady-state" burning (i.e., effect of initial transients is washed out) is achieved in 700 single processor hours.

3.1 Sandwich Propellant Combustion

Three configurations are studied here to get a better understanding the nature of flame structure near the surface as the AP-binder scales are changed. A gas phase computational domain of 0.4 mm in the streamwise (x) and 0.8 mm in the transverse (y) direction is resolved using a grid resolution of 200 x 240. The solid phase has a depth of 0.16 mm. The grid is uniform in the streamwise direction with a grid spacing of 2 μm while the grid is stretched in the transverse direction such that in the AP-binder region the resolution is also 2 μm while near the periodic boundary it approaches 6 μm. The typical schematic grid distribution is shown in Fig. 4. For all cases studied here, the pressure was 20 bar.

The three cases differ in the sandwich packing between AP and binder: (a) a single slice of binder of 100 μm with AP on both sides, (b) a single slice of binder of 40 μm, and (c) three slices of binder of 60, 40 and 60 μm separated by two slices of AP of 40 μm.

Some characteristic results are discussed below. For the 100 μm single binder slice case, Figs. 5a-c present respectively, the temperature field, the AP decomposition reaction rate and APd-binder reaction rate contours. The temperature field has a maximum temperature of 2600 K. Multiple flame structures can be seen in this figures. For example, the APd-binder reaction rate contours (Fig. 5c) show the flame front for the reaction between the AP decomposition products and the binder. The upper side of this flame is a non-premixed flame since diffusion of both species is required to initiate reactions. On the other hand, the lower side is a premixed flame (as it will be proved later). The horizontal reaction rate contours (Fig. 5b) show the flame zone due to the AP decomposition reaction. Both flames are coupled together at the interface between AP and binder.

Figures 6(a) and 6(b) show respectively, the axial and tangential velocity components in one-half domain near the AP/binder interface. The highest velocity gradients are in the flame region due to thermal expansion. The tangential velocity component has the largest value at the AP/binder interface, above the surface. Although the regression rate is almost the same for AP and binder at the interface, the solid AP density is more than twice the solid binder density (1950 to 920 Kg/m3). Thus, the velocity of the AP gas is twice the velocity of the binder at the surface. This high speed (which is normal to the AP surface) is inclined inwards near the AP/binder interface and results in an effective convergence of the flow from both sides due to the aforementioned increase in the tangential velocity. The resulting flow pattern is shown imposed over the APd-binder reaction rate contour in Fig. 7.

By computing the mass flow rate for each species with both convective and diffusion effects, the path of AP and binder though the gas phase can be obtained and is presented in Fig. 8 (a) and Fig. 8 (b), respectively. It can be seen that in the near surface region, the convective effect is dominant whereas, close to the APd-binder reaction zone this effect is overcome by the diffusive effect. The concentration of the reactants behind the reaction zone are extremely small (between 0.0001 right after the reaction and 10^{-9} at the end) so the streamlines after the high reaction correspond to insignificantly small quantities of APd (respectively binder).

The thickness of the diffusion flame (the distance between the two location of the medium reaction rate) has been recorded for several positions. All the values were around 20 μm (15 μm in the premixed zone and 22 μm in the diffusion region). For the AP flame the thickness increased from 13 μm in the high reaction rate region to 35 μm far from the diffusion flame.

When the final "steady" burning shape is reached, the AP surface near the AP/binder interface is extremely inclined and the tangential velocity component is more than 50% of the incoming AP gas jet. This component therefore, determines the flame position. As the slope of the surface at the interface becomes steeper, the flame moves from the interface above the binder. Only in the transient phase, when the surface is flatter, the highest regression rate is in the AP grid cell closest to the binder. After that the flame moves away from this position and stabilizes on the top of the binder. This increases the effective heat transfer to the binder and as a result, the binder has the highest regression rate. This is different from what has been observed experimentally.[6,7] The computed features of the flame are consistent with the observation but the regression rate (about 10 mm/s) is about twice the experimental value (4 mm/s).[6] The discrepancy in shape may be due to the global mechanism employed. The right regression rate can be achieved with a suitable choice of the parameters in the Arrhenius rates. We revisit this case below to demonstrate the sensitivity of the prediction to the parameters in the kinetics model.

When the binder width is small, the 40 μm case, the surface of the binder is almost flat and slightly below the interface due to heat conduction to the colder AP. The temperature, the AP decomposition reaction rate and APd-binder reaction rate contours are shown in Figs. 9a-c, respectively. Other features are qualitatively similar and therefore, are not repeated here for brevity.

The temperature contours inside the computational domain (the gas and the solid phase) are shown in Fig. 9 (a). The highest temperature in the gas field is above the binder, in between the two diffusion flames. The highest gradients are in the premixed reaction zone. In the solid phase the surface temperature is higher in the binder even though the conductivity of the binder is smaller than the AP conductivity (0.276 W/mK and 0.405 W/mK). The reason is that the heat flux is larger above the binder (the flame sits on top of it!) and also the sublimation heat is lower for binder (2.0×10^5 J/Kg versus 4.2×10^5 J/Kg for AP). The gradient is steeper in the binder due to the lower conductivity.

Comparing the reaction rates and the concentrations, it is noted that the fastest reaction for the APd-binder reaction occurs in a premixed mixture (fuel and oxidizer in equal proportions), decreasing for the leaner and the richer

mixtures. In order to visualize better the limits between the premixed and diffusive flames, in Fig. 10, the double lines are used to identify a stoichiometric mixture within 0.5% ($[b] * \beta/[APd]) \cong 1$ where $\beta = 8$ is the stoichiometric coefficient, [b] is the binder concentration and [APd] is AP decomposition products concentration). In this figure, the contours represent the APd - binder reaction rates. The location where the slope of the stoichiometric mixture changes and the maximum reaction rates shifts away from the stoichiometric mixture may be considered the beginning of the premixed flame. The whole flame above the limit line is stoichiometric within 5% (so it is a diffusion flame). The maximum reaction rate for the diffusion flame occurs for the concentration closest to stoichiometric surface (the double lines) slightly toward the richer mixture. The regression rate in this case is 9.5 mm/s and the maximum temperature is 2665 K.

The three-binder case shows interesting behavior of flame interactions. The APd-binder flames seated right above the AP slices (premixed flames) have the same behavior as the single slice for the external diffusion flames and the overall temperature contours show similar trends as in the single binder case (Fig. 11a). For the thin AP slices, the AP decomposition products are consumed as soon as they are produced (Figs. 11(b) and 11(c)) because the binder is in excess. The reaction is very fast, so the APd-binder flame has to be a premixed flame above the thin AP slice.

Since both the 40 and the 100 μm cases discussed above predicted higher regression rates than was measured in the experiment, another case of the 40 μm have been performed with slightly modified parameters for the AP decomposition and the AP decomposition products-binder reaction. The new parameters are:

$D_1 = 0.4 * 2.234 \times 10^7$; $n_1 = 1$; $E_1/R_u = 8000K$

$D_2 = 0.1 * 1.105 \times 10^7$; $n_2 = 1$; $E_2/R_u = 11000 + 100K$

These changes had a remarkable result. The stand-off distance for the APd-binder flame increases and the premixed and the diffusive reactions merged together, as shown in Fig. 12. The maximum temperature drops to 2400K and the regression rate is 3.7 mm/s, which is very close to the observed value.[6] Furthermore, this case also shows that the AP surface is leading the burning surface, as in experiments[6] and the surface is much flatter than in the previous case. The stoichiometric mixture is also shown in Fig. 12 (the double line) and this suggests that the reaction is occuring mostly in the premixed state.

The sensitivity of the flame structure and regression of the burning surface to slight changes to the kinetic rates in the reaction model highlight the need for a more comprehensive data base for the reaction mechanism and the relevant rates if the physics of propellant combustion is to be properly resolved. However, the DNS capability developed here demonstrates that subtle changes in the flame structure can be captured with spatial and temporal accuracy and therefore, this capability can be exploited to anchor global mechanisms to measured data as well. Parametric studies can also be conducted to determine the impact of different sandwich preparations. If and when properly validated mechanisms become available such features can be easily incorporated in this code since it allows for arbitrary number of species and reaction kinetics.

3.2 Random Packed Propellant

A more realistic propellant preparation is a randomly packed AP in a binder base. Typically, the AP particles are of random 3D shapes of various sizes. In the present study we consider random packing of AP cylinders of various diameters. The computational gas phase domain of $x = 0.8$ mm and $y = 0.36$ mm with a solid phase depth of 0.2 mm is discretized using a 400 x 180 uniform grid in both directions so that the smallest scale resolved is a 2 μm square. A typical domain and random packing is shown in Fig. 13.

The package is generated by randomly placing the center of the AP particles in the solid domain, initially occupied only by the binder. In order to avoid overlapping, first the domain assigned to the particles is checked and if another particle is already there, the center is moved to the next grid point. The number of grid cells occupied by each species is counted to obtain the required volume fraction (in a stoichiometric case, AP/binder: 80/20 by volume).

The gas flow, the surface shape and the reactions are tightly coupled in this case. The characteristic reaction time and the characteristic flow time are of the same order of magnitude ($8x10^{-10}$ sec.). The streamlines in Fig. 14 show how the gas comes out normal to the surface and then is diverted by the APd-binder reaction, and the accompanying heat release induced volumetric expansion.

Figures 15 (a) and (b) show respectively, the AP decomposition and the APd-binder reaction locations and magnitude. The AP decomposition flame thickness is almost constant above the surface. Due to the nature of the packing, the APd-binder flame has a premixed component above the surface and some diffusive branches. This type of mixed flame structure is likely to be related to the characteristic length scales between the various AP particles and the intermediate binder. A careful parametric study is planned to determine how the flame structure changes from diffusion type to a fully premixed type. These results will be reported in the near future.

A time sequence of the surface burning and regression along with the flame structure is shown in a time series in Figs. 16a-h. In this sequence it can be seen that the diffusion flame has an on-off-on behavior due to the burning at the packing surface. This is related to the change from the diffusion flame to the premixed flame when the AP/binder interfaces are replaced by pure AP boundary. The ability of the DNS code to capture this sort of rapid changes in the flame structure points to the ability developed in this effort.

Compressibility effects are shown in Fig. 17. For a temperature range of 900 K to 2700 K and a pressure p = 20 bar, the density is between 3 and 9 Kg/m^3. The plots show density variation along line 1 (streamwise), line 2 (tangential), and line 3 (streamwise in the flame region). For higher

pressures the gradients will be larger.

4 Conclusions

A 2D DNS code to simulate solid propellant combustion with fully coupled gas-solid phase has been developed. Many different types of packing including sandwich and random packing with arbitrary AP particle size can be simulated with this code. Although a global kinetics model is employed at present, the current code has the capability to deal with any type of kinetics. Parallel implementation has allowed very fast calculations with very fine resolution of the flame zones. It has been shown here that the flame structure above the surface is a combination of lean-rich premixed and diffusion flames and the state can rapidly change as the surface regresses (especially in the randomly packed case). For the sandwich case, it has been shown that the surface regression rate is very sensitive to the global kinetics parameters employed and this suggests the critical need to get a better reaction kinetics model for this type of combustion.

Acknowledgments

This research is supported by the Office of Naval Research with Dr. Judah Goldwasser as the Program Manager. The computational time was provided by DOD HPC Center at NAVOCEANO and ERDC, MS. Many helpful discussions with Dr. J. Seitzman must also be mentioned.

References

[1] Hegab, A., Jackson, T. L., Buckmaster, J., and Stewart, D. S., "Nonsteady Burning of Periodic Sandwich Propellants with Complete Coupling between the Solid and the Gas Phases," *Combustion and Flame*, Vol. 125, 2001, pp. 1055–1070.

[2] Jackson, T. L., Buckmaster, J., and Stewart, D. S., "Heterogenus Propellant Combustion," *AIAA Journal*, Vol. 40, 2002, pp. 1122–1130.

[3] Kim, W. W., Menon, S., and Mongia, H., "Large-Eddy Simulation of a gas Turbine Combustor Flow," *Combustion Science and Technology*, Vol. 143, 1999, pp. 25–62.

[4] Poinsot, T. J. and Lele, S. K., "Boundary Conditions for Direct Simulations of Compressible Viscous Flows," *Journal of Computational Physics*, Vol. 101, 1992, pp. 104–129.

[5] Yang, G., Causon, D. M., and Ingram, D. M., "Cartesian Cut-Cell Method for Axisymmetric Separating Body Flows," *AIAA Journal*, Vol. 37, 1999, pp. 905–911.

[6] Price, E. W., Sambamurthi, J. K., Sigman, R. K., and Panyam, R. R., "Combustion of Ammonium Perchlorate-Polymer Sandwiches," *Combustion and Flame*, Vol. 63, 1986, pp. 381–413.

[7] Price, E. W., "Effect of Multidimensional Flamelets in Composite Propellant Combustion," *Journal of Propulsion and Power*, Vol. 11, 1995, pp. 717–728.

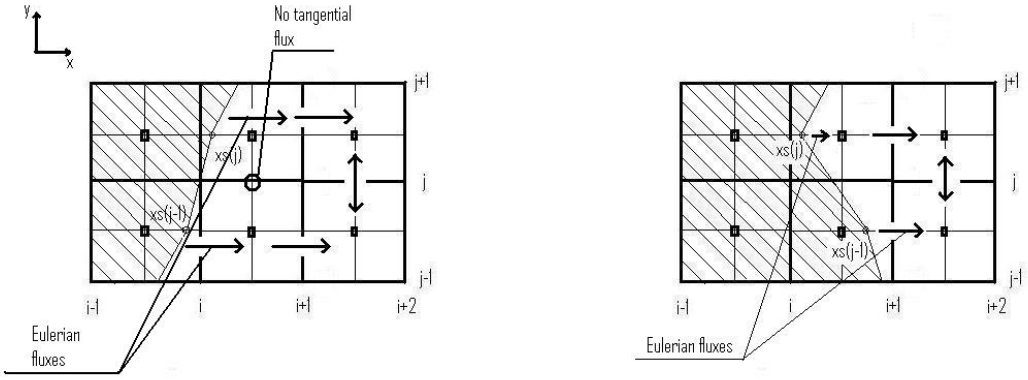

a) **b)**

Figure 1 The surface fluxes for two surfaces. If a fluid cell has a neighbour containing the surface, the tangential flux between those two cells is not computed.

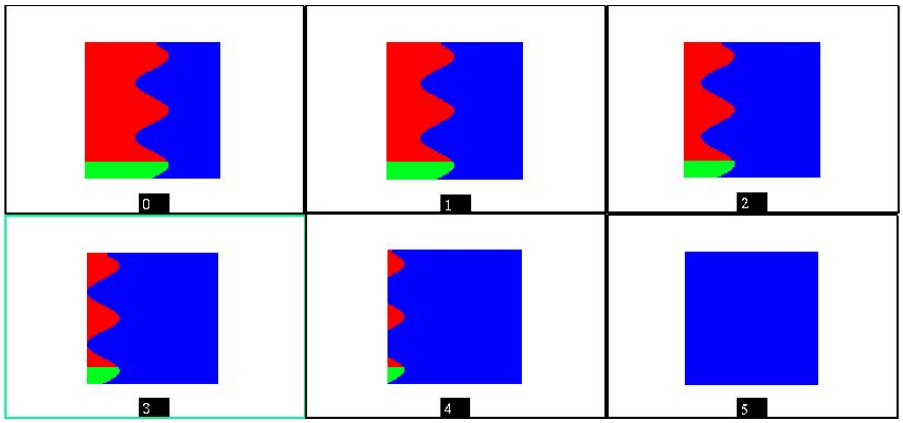

Figure 2 Movement of a sinusoidal surface at a fixed speed through the stationary grid. Surface remains undistorted and moves at the same speed on all points at the surface. This demonstrates the accuracy of the regression model.

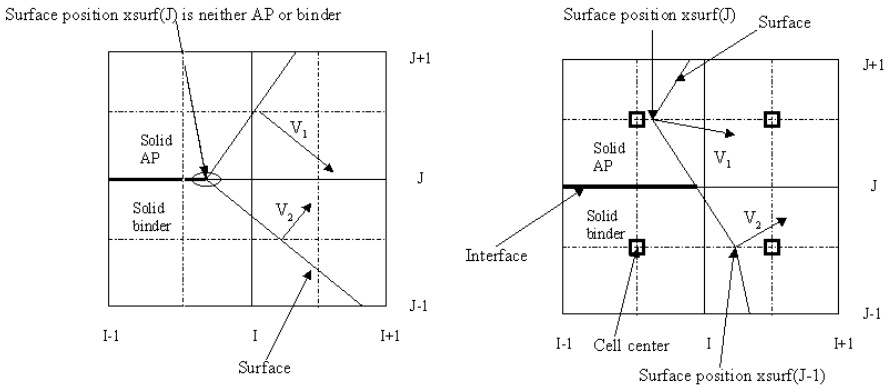

a) **b)**

Figure 3 (a) Velocities from AP and binder have opposite sign. If the surface is tracked using the intersection with the grid then the regression rate at the interface AP/binder would be undefined (b) Velocity direction is an average of the two normals.

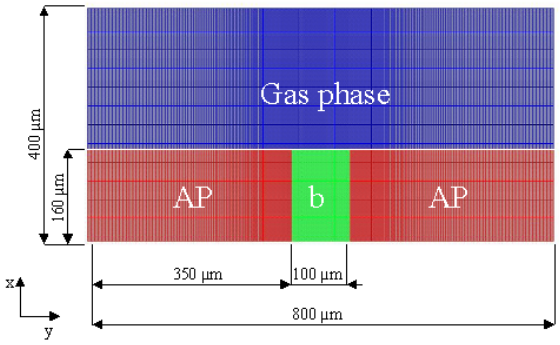

Figure 4 Computational domain used for various sandwich simulations. The length of the gas domain is 400 μm **and the width is** 800 μm**. The length of the solid subdomain is** 160 μm**.**

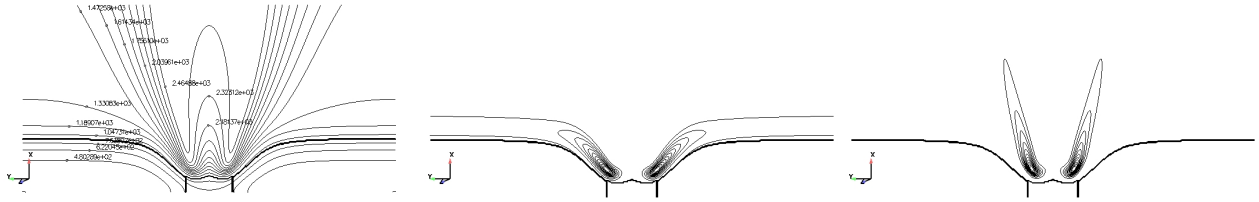

a) b) c)

Figure 5 Temperature and reaction rates contours for the 100 μm **case. (a) Temperature; (b) AP decomposition reation rates; (c) AP - binder reaction rates.**

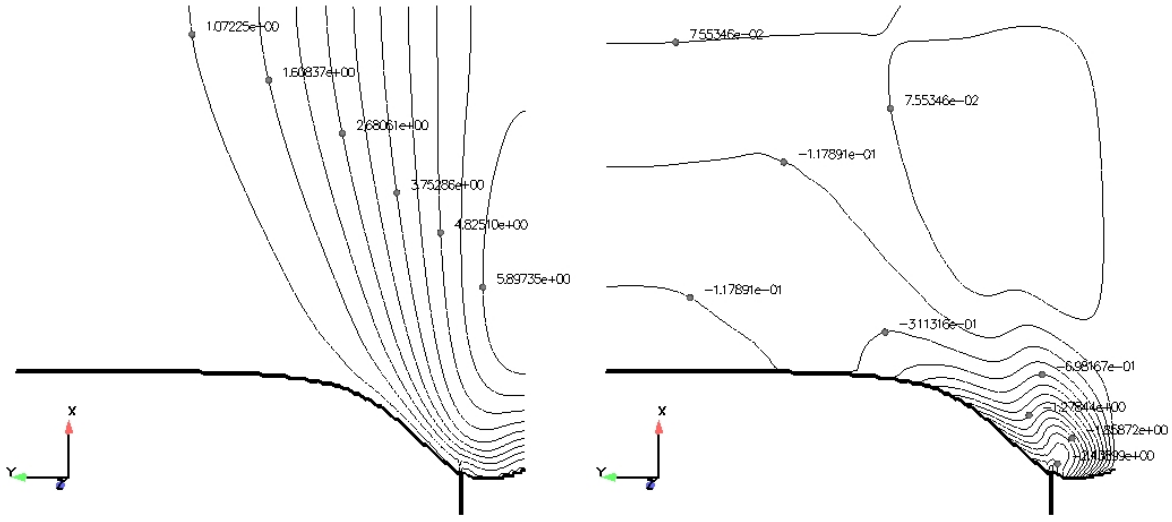

a) b)

Figure 6 Velocity components (in m/s) near the solid surface. Only one-half of the domain is shown for clarity. (a) Axial (x-) velocity component and (b) Tangential (y-) velocity component.

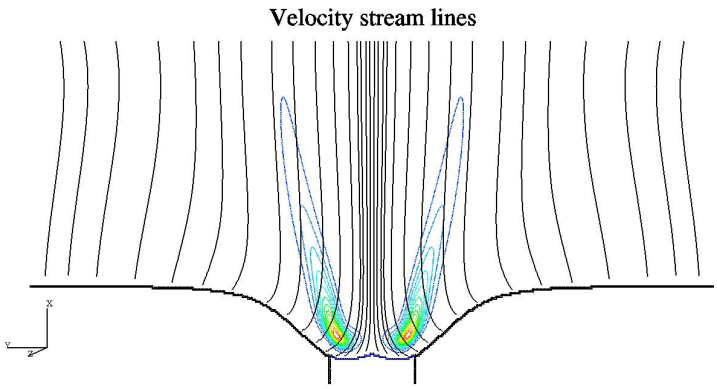

Figure 7 Streamline pattern near AP-Binder Interface. Also shown is the APd-binder reaction rate contours.

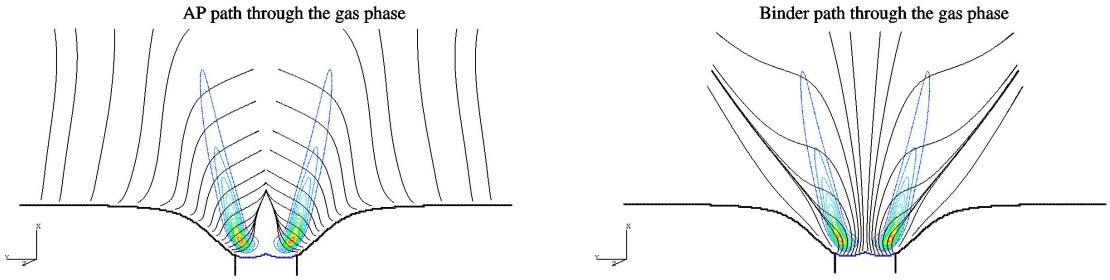

a) **b)**

Figure 8 Mass flow of gases from AP and binder. (a) AP gas motion, (b) Binder gas motion.

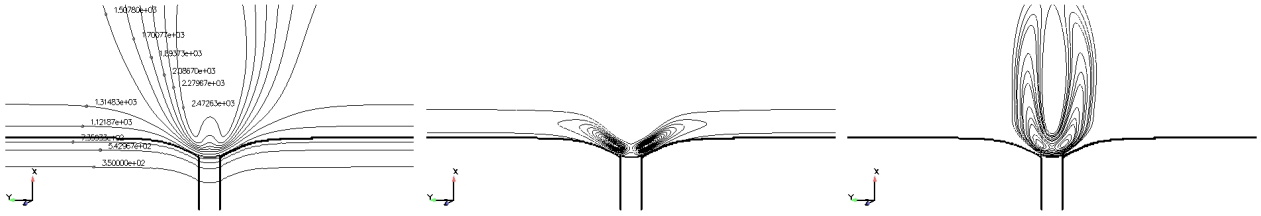

a) **b)** **c)**

Figure 9 Temperature and reaction rates contours for the 40 μm **case (a) Temperature; (b) AP decomposition reation rates; (c) APd - binder reaction rates.**

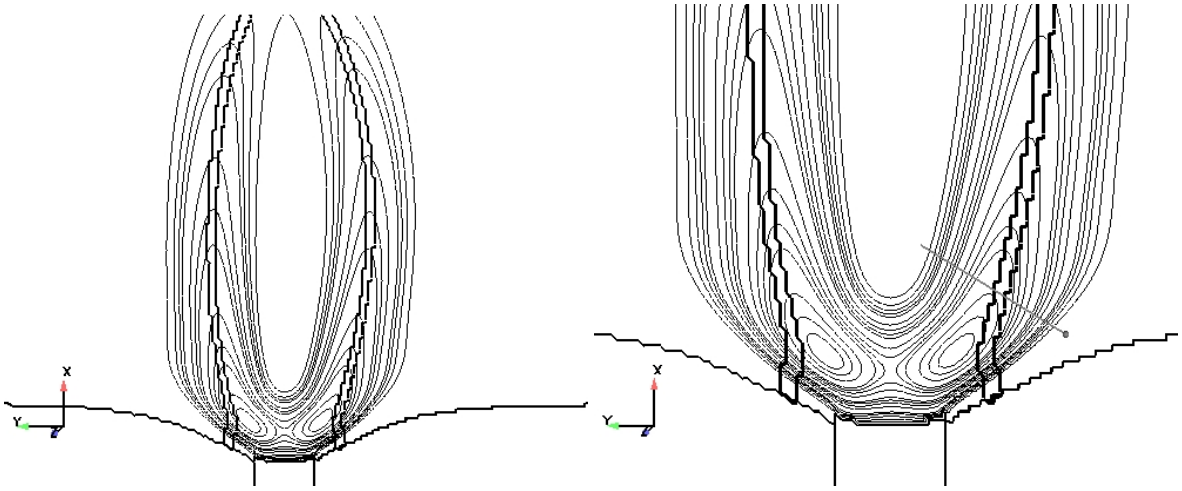

a) b)

Figure 10 (a) The structure of APd-binder flame. The double line is stoichiometric mixture and the contours are reaction rates for APd/binder reaction rates; (b) Detail: The line is the limit between diffusive and premixed flames.

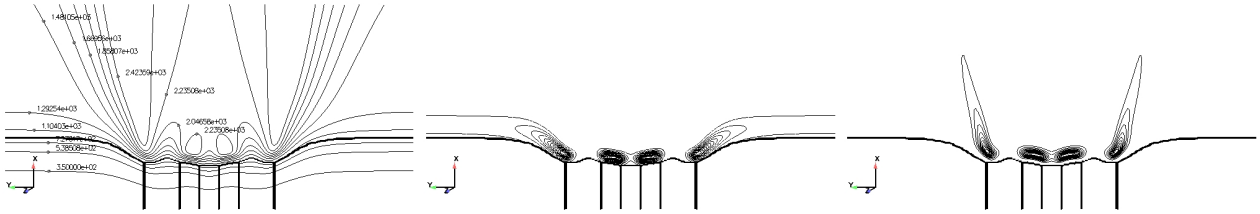

a) b) c)

Figure 11 Temperature and reaction rates contours for the three-slice case (a) Temperature; (b) AP decomposition reation rates; (c) APd - binder reaction rates.

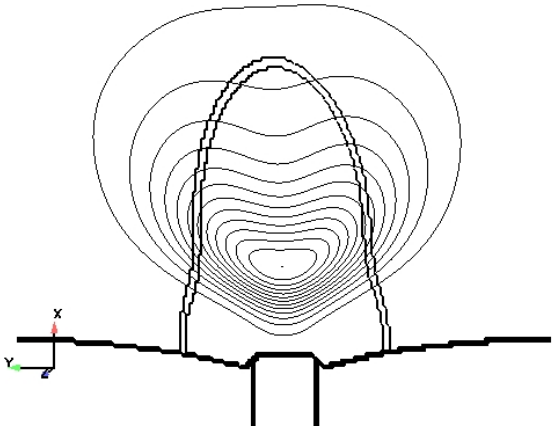

Figure 12 For a lower reaction rate, the premixed and diffusive flames merge together an the stand-off distance increases. The AP is leading the regression. The double line shows the stoichiometric mixture.

Figure 13 Computational domain for random packing (the circles are AP particles with binder in between, the dark color is the gas phase). The package consists of AP particles of 10, 30, 40 and 80 μm embedded inside a binder.

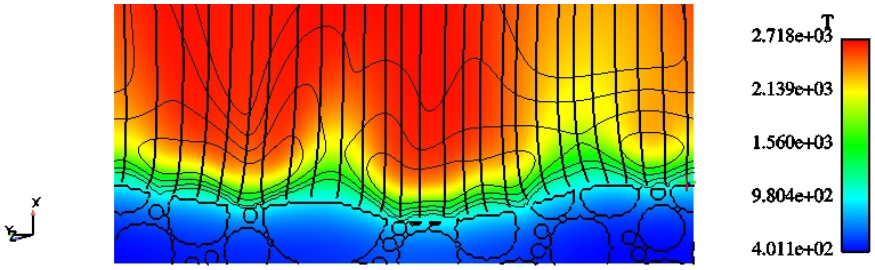

Figure 14 Temperature and reaction rate contours for a random package. The vertical lines are the streamlines, contours are APd/binder reaction rates, and the colors represent the temperature field (K). In the solid region the circles are AP particle boundaries.

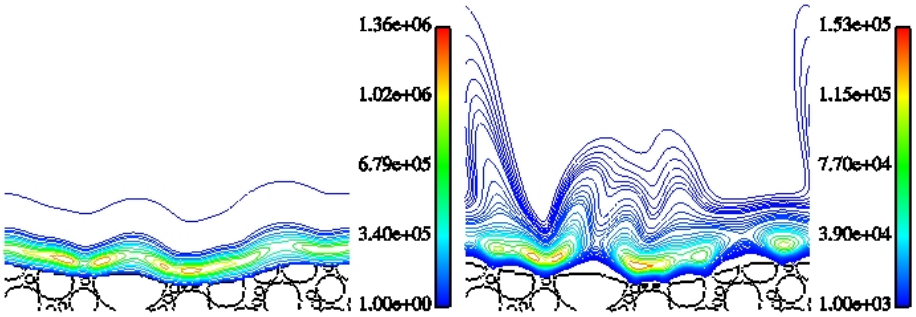

a) **b)**

Figure 15 Reaction rates contours. (a)AP decomposition flame and (b) Apd-binder flame.

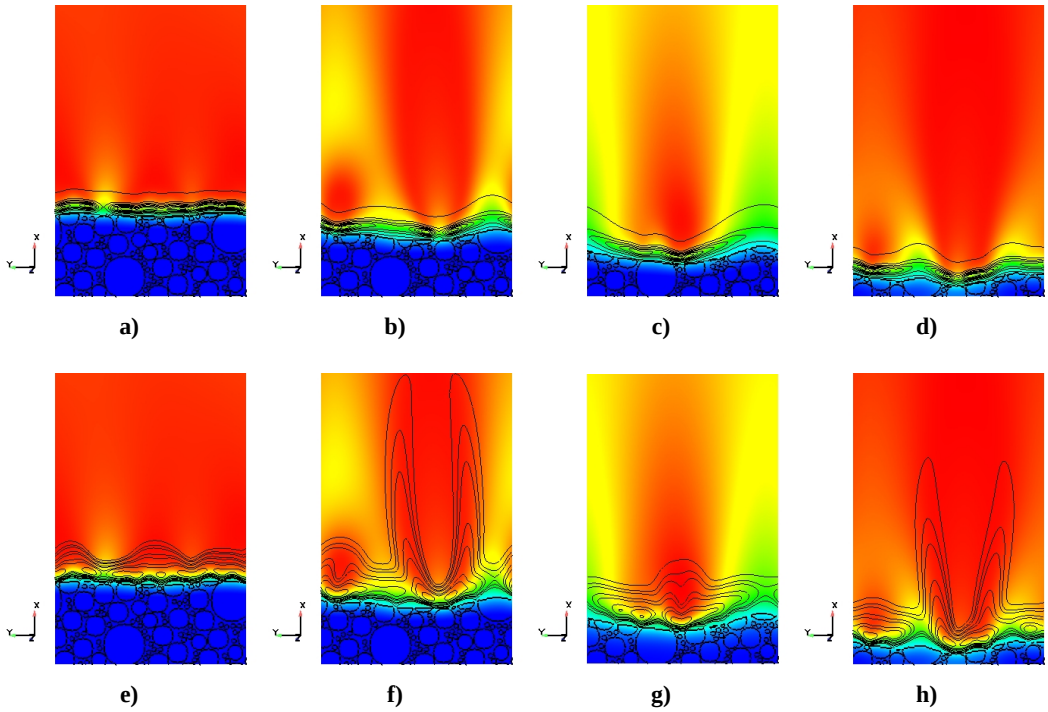

Figure 16 Reaction rates contours and temperature field at four instants in time. The top sequence shows the AP decomposition contours. The bottom sequence shows the APd/binder reaction contours. The colors represent the temperature (same scale as in Fig. 14). (a),(e) t = 0.0044 s; (b),(f) t = 0.0088 s; (c),(g) t = 0.0132 s; (d),(h) t = 0.0176 s.

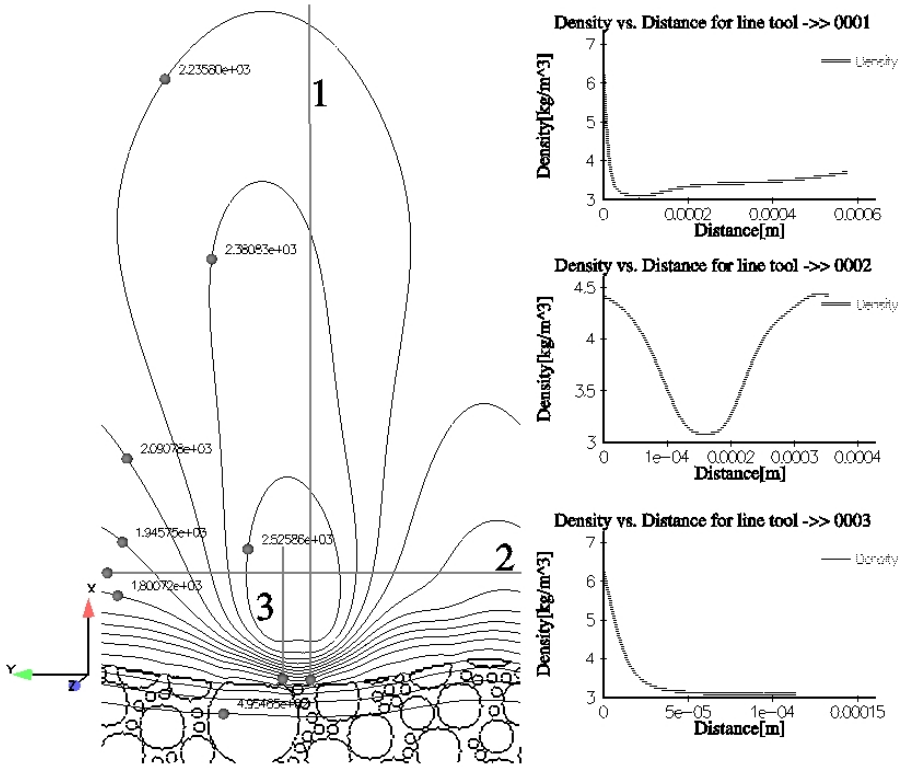

Figure 17 Compressibility effects. The plots show the density variation along lines 1 (streamwise), 2 (tangential), 3 (streamwise in the flame region). The contours show the temperature distribution.